Nano3D

Project no. NMP4-CT-2005-014006

Project acronym: NANO3D

Project title: Precision Chemical Nanoengineering: Integrating Top-Down and Bottom-Up Methodologies for the Fabrication of 3-D Adaptive Nanostructured Architectures

Instrument: Specific Targeted Research Project

Priority Three: NMP

PUBLISHABLE SUMMARY

Period covered: from 1/6/2005 to 30/9/2008
Date of preparation: October 2008

Start date of project: 1/6/2005 Duration: 40 months

Project coordinator name: Professor Jon A Preece
Project coordinator organisation name: The University of Birmingham

Project objectives

The overall objective of the project was to integrate top-down lithographic techniques which enable precise spatial patterning of surfaces from micron- to the nanoscale, with the controlled stepwise self-assembly and self-organisation of nanometre scale chemical and biochemical entities to these surfaces, to fabricate three dimensional adaptive nanostructured architectures.

A schematic of the project is shown below, starting from a bare substrate, moving through to functionalisation of surfaces, patterning, build-up of structures progressively into the third dimension, and finally adding the 'roof ' structure (stage 6).

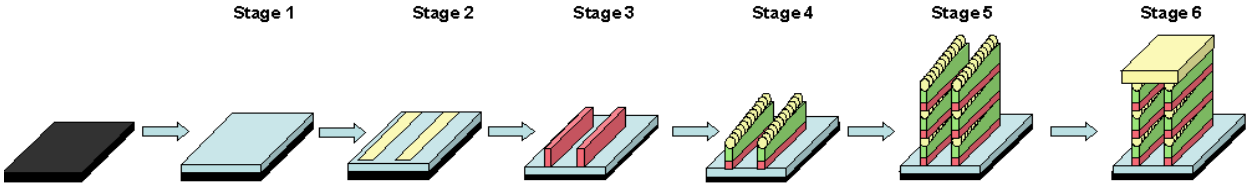

Schematic of the Nano 3D project.

To achieve the project objectives, the work programme was split into work packages addressing *molecular foundations, building blocks, adaptive architectures,* and *scale-up.*

Partners involved

University of Birmingham, UK (Coordinator) (UB)
Tyndall National Institute, Cork, Ireland (TNI – UCC)
Max Planck Institute for Polymer Research, Mainz, Germany (MPIP – MPG)
Consejo Superior de Investigaciones Cientificas, Barcelona, Spain (CSIC)
BAE Systems Advanced Technology Centre, Bristol, UK (BAE)
9D Technologies, Marly, Switzerland (9D)

Work performed and end results

The challenging project objectives have largely been met. Key research highlights are summarised below:

- Nanoscale patterning of self-assembled C_{60} adducts and citrate passivated gold nanoparticle structures (UB)

- Micro-scale patterning of hairpin oligonucleotides bearing photolabile groups using UV-photolitography, and the specific deposition of gold nanoparticles on surfaces mediated by DNA. This is one of the first demonstrations of the use of DNA-bearing photolabile groups to obtain patterns on silicon oxide surfaces (CSIC and UB)

- A polymer nanowire photodetector with potential for applications in nanoscale building blocks for future hybrid nanophotonic devices and systems (TNI-UCC)

- An optically pumped single nanowire laser (TNI-UCC)

- Formation of, and substrate-adaptive behaviour in integrated micron-scale "wall + roof" structures comprising blends of hydrogels and nanocrystals (UB & MPIP-MPG, with fabrication assistance from TNI-UCC)

- Ink-jet deposition of wall and roof microstructures on silicon oxide substrates (9D and UB)

- Microfluidic scale-up route for formation of wall structures based on UB's process route of sequential deposition of nanoparticle- and polyelectrolyte layers (BAE and UB)

- Strong dissemination of results throughout the project (both published articles and presentations). Published work included three journal cover articles, indicative of the high quality of the research output.

Certain aspects of the project will require further development, especially the more structurally complex (stage 6 in the project schematic above) and in particular some aspects of the *adaptive nature* of such structures.

The key research highlights given above are now addressed in more detail.

MOLECULAR FOUNDATIONS

There have been a number of materials developed in the category of molecular foundations, including self-assembled monolayer structures, gold nanostructures of various types, polymer nanowires and silane derivatives for silica surface functionalisation.

The examples highlighted here describe the development of materials based on C_{60} and thiol passivated gold nanoparticles. These can form the basis of non-adaptive walls. In the first development, the C_{60} can be used in the scanning near field photolithography (SNP) process, whereby Langmuir-Blodgett films of an amphiphilic C_{60} moiety are transferred to SiO_2 substrates and written to by a scanning near field optical microscope (SNOM), which induces photochemical cross-linking, either through cycloaddition reactions of adjacent π-units or allene formation (***Figure 1a***). ***Figure 1b*** and ***figure 1c*** illustrate that the resulting walls are 50 nm in width and about 4 nm high (SNOM writing speed of 2 μm s^{-1}). It was observed at slower writing speeds that the wall width and height dimensions were larger, presumably because the longer dwell times increased the degree of cross-linking. Careful inspection of ***figure 1b*** reveals that there are some much thinner, but incomplete, walls with a width of about 10 nm. These walls are formed at writing speed of 35 μm s^{-1}. This provides a methodology for controlling the dimensions of these walls.

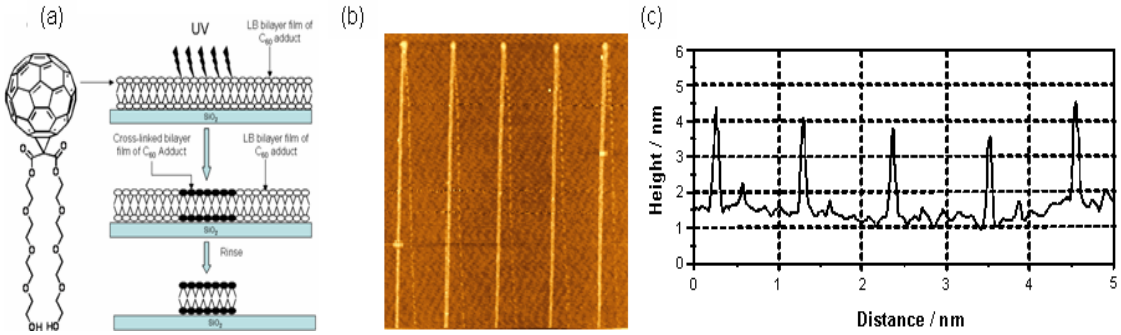

Figure 1. (**a**) C_{60} derivative and processing steps, (**b**) AFM micrograph of the pattern after rinsing (step height (3 nm, 1 bilayer), and (**c**) cross section analysis.

The second method, involving the fabrication of gold nanowalls on SiO_2, used the deposition of Langmuir-Schaeffer films of thiol passivated gold nanoparticles (***figure 2a***) on SiO_2 and then writing to the films with the SNOM. The SNOM induces a photochemical oxidation of the thiolate to sulfonate (***figure 2b***), which only bind weakly to the gold particles, allowing the particles to aggregate (***figure 2c***). Rinsing the surface washes away the unirradiated gold nanoparticles (***figure 2d***), to afford 50 nm gold walls (***figure 2e***). The height of the wall can be controlled by the number of layers of the gold particles transferred and by the SNOM writing speed.

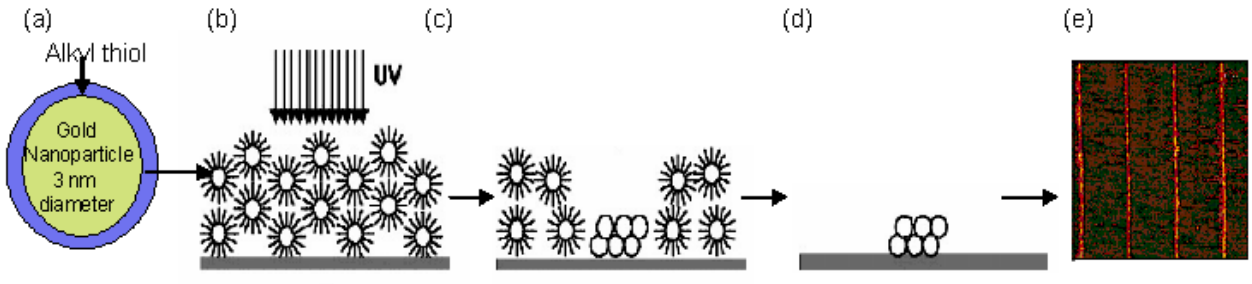

Figure 2. (***a***) Thiol passivated gold nanoparticle, (***b***) UV exposure (***c***) depassivation of thiols from particles, (***d***) rinsing, and (***e***) AFM topographical image the gold nanowires (50 nm wide lines, 6 nm high).

BUILDING BLOCKS

Functional Oligonucleotides

CSIC synthesised nucleic acid derivatives with a hairpin structure having two functional groups: (i) a classical anchoring group such as amino or thiol group as well as azido or alkynyl groups and (ii) a photolabile group (A group with a bond capable of being broken by light irradiation). The anchoring group was needed for the immobilization of oligonucleotides on surfaces. A photolabile group was later added in the loop of the hairpin. In this way and, after immobilization of the hairpin to the surface, light was used to break the photolabile bond at the loop. In this way the half of the hairpin washed out and the parts of the surfaces that had been irradiated contain single-stranded oligonucleotides. The single-stranded regions were selectively addressed by the complementary strand which allowed the immobilization of new molecules or nanomaterials at specific sites. ***Figure 3*** shows a schematic of the process with the photocleavable hairpin DNA self-assembled monolayers (SAMs).

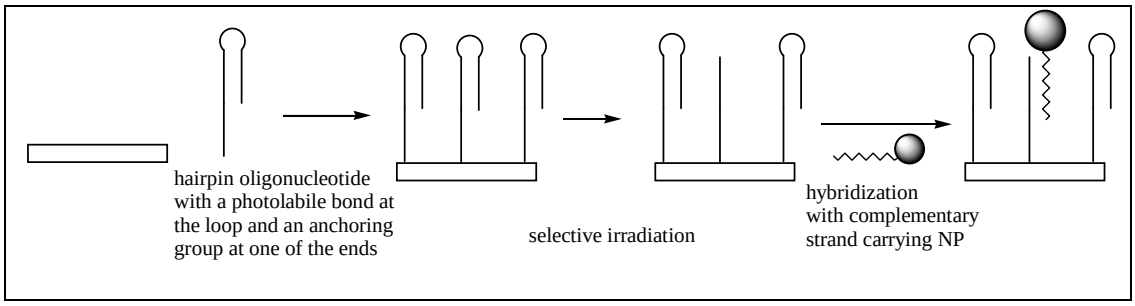

Figure 3. Schematic of photocleavable hairpin DNA self-assembled monolayers

SAMs functionalised with hairpin oligonucleotides were fully characterised by AFM, contact angle measurements and ellipsometry. The photolysis of SAMs functionalised with the hairpin oligonucleotide yielded a SAM functionalised with a single stranded oligonucleotide, observing the disappearance of the double-stranded DNA molecules by AFM. The addition of the complementary DNA sequence labelled with rhodamine dye yielded the expected rhodamine-labelled SAM and the recovery of the double-stranded DNA molecules on the SAM was visualized by AFM (see ***figure 4***).

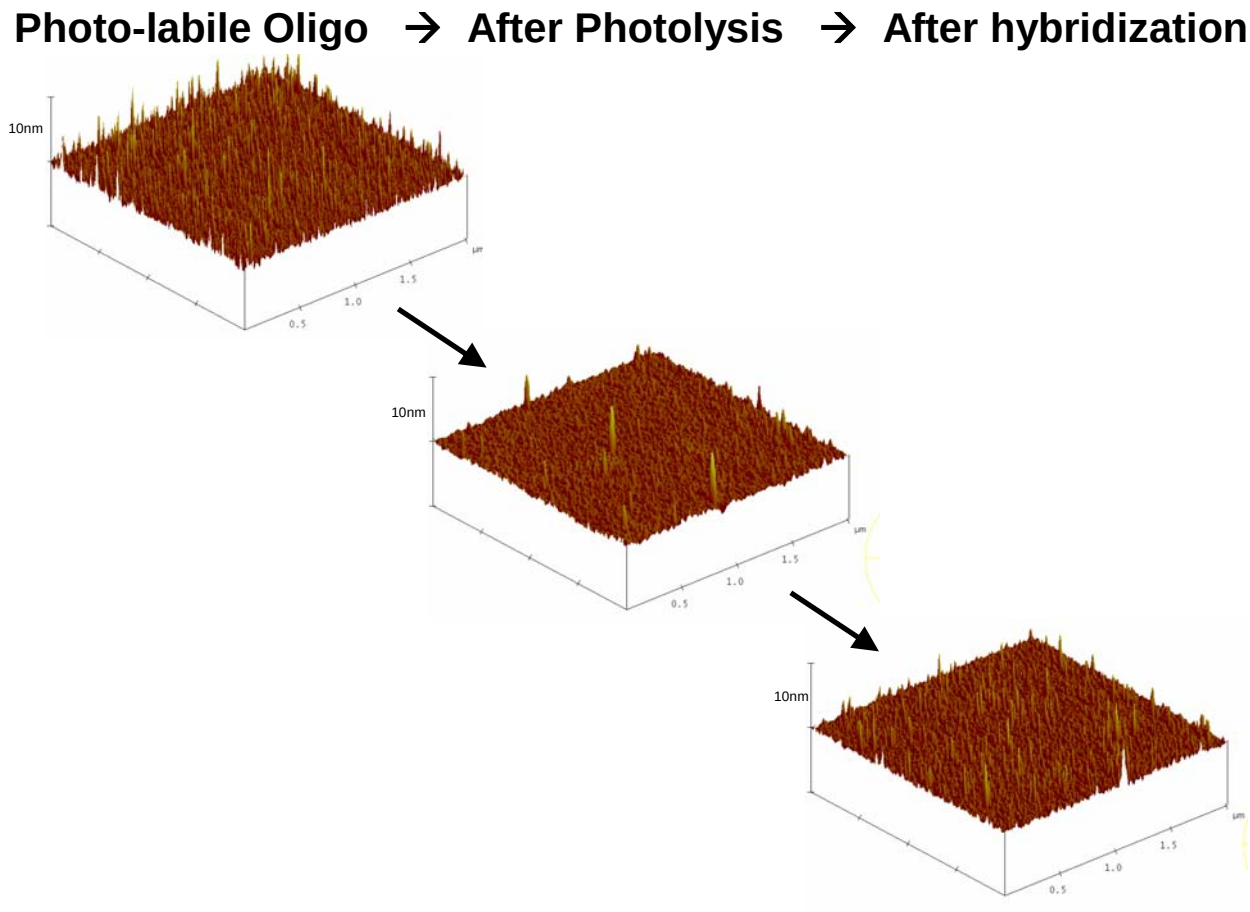

Figure 4. AFM images of photolabile oligonucleotide, before and after photolysis and after hybridization.

Figure 5 shows the scheme and results of the photolithographic process using the photolabile hairpin DNA. Oligonucleotide hairpin sequences were attached to the silicon oxide surface using self-assembled monolayers (SAMs) functionalized with isothiocyanate groups. Photolysis of the oligonucleotide layer and subsequent hybridization of either the complementary oligonucleotide sequence labelled with rhodamine, or else gold nanoparticles carrying a complementary sequence, was employed to develop routes to active wall structures. The upper image shows the wall microstructures obtained with rhodamine-labelled oligonucleotides visualized by epifluorescence. The image below shows the patterning obtained with oligonucleotide-bearing gold nanoparticles.

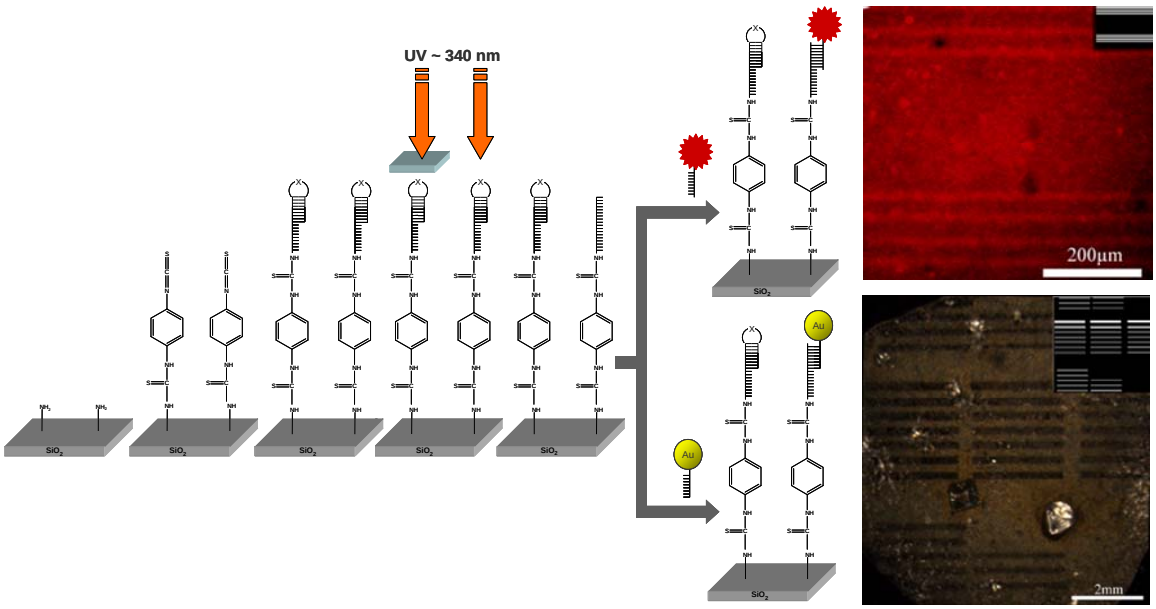

Figure 5. (a) photolabile hairpin DNA scheme, with the resulting patterned (b) rhodamine labelled oligonucleotides (upper) and oligonucleotide-bearing gold nanoparticles (lower).

To summarise, CSIC has achieved the patterning of SAMs with hairpin oligonucleotides carrying photolabile groups using a micrometer size mask and UV-photolitography. In addition, the specific deposition of gold nanoparticles linked to oligonucleotides on surfaces with single-stranded oligonucleotides generated by p
hotolysis of hairpin oligonucleotides carrying photolabile groups has been achieved.

Polymer Nanowire Photodetector

Tyndall developed photoconductive nanowires, synthesised from poly[(9,9-dioctylfluorenyl-2,7-diyl)-co-(bithiophene)] (F8T2) via a solution-assisted template wetting method. Individual F8T2 nanowires were electrically interfaced using either bottom or top-contact geometries; see ***figures 6.1 & 6.2***. Current-voltage characteristics acquired for bottom-contacted single nanowire devices indicated barrier formation at the nanowire-electrode interface and the range of the measured resistivity values, 7. 10^3 Ωm < ρ < 4. 10^4 Ωm, indicated (unintentional) doping, possibly arising from air exposure; see ***figure 6.1***. Single nanowire photoconductivity measurements were performed using a modified near-field scanning optical microscope. Top-contacted single nanowire devices with interelectrode gaps ~ 5 µm were fabricated on glass substrates using shadow masking and gold evaporation; see ***figure 6.2***. The blue curve in ***figure 6.2b*** shows the measured dark current (I_{dark}) for a typical device. The data shows quasi-linear characteristics at low bias, similar to measured data for bottom-contacted nanowires, with some asymmetry at higher bias. The red curve in ***figure 6.2b*** shows the measured current (I_{illum}) under continuous 405 nm illumination. A marked increase in the measured current is observed across the entire bias range. The green

curve in ***figure 6.2b*** shows the measured current under manually chopped 405 nm illumination, where the illumination was switched on or off at 10 V intervals during the bias sweep, corresponding to a duty cycle of 50%. These data demonstrate almost complete recovery of the device after illumination is removed, indicating that the photocurrent response is significantly larger than any thermionic or thermoelectric effects that might arise from a photo-induced temperature increase.

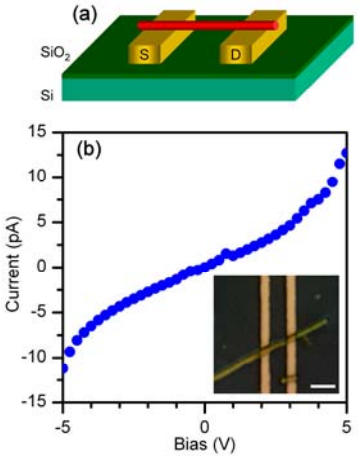

Figure 6.1 (a) Schematic of a bottom-contact nanowire device. (b) I-V characteristics of a bottom contacted F8T2 nanowire acquired in the dark. Inset: Optical micrograph of this device. Scale bar: 2 μm.

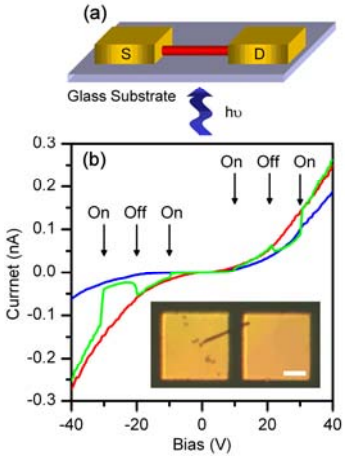

Figure 6.2 (a) Schematic of a top-contact nanowire device. (b) Current-voltage (I-V) characteristics of a top-contacted F8T2 nanowire acquired in the dark (blue line) and under 405 nm illumination (red line). Reversible switching in I-V data measured under manually chopped 405 nm illumination is also shown (green line). Inset: Optical micrograph of a typical top-contacted F8T2 nanowire device. Scale bar: 10 μm.

This work resulted in a publication in *Advanced Materials* with journal cover graphics: O'Brien, G.A.; Quinn, A.J.; Tanner, D. & Redmond, G. "*A Single Polymer Nanowire Photodetector*" *Adv. Mater.* 18, *2379* (2006).

The photocurrent can be defined as $I_{ph} = I_{illum} - I_{dark}$. A useful figure of merit for photodetectors is responsivity (R_{res}), the ratio of the photocurrent to the incident light power. The responsivity can be calculated from $R_{res} = I_{ph} / I_{irr} A$, where A is the effective device area and I_{irr} is the irradiance of the incident light. The measured single nanowire responsivity for the device with data shown in ***figure 6.2b*** is R_{res} = 0.4 mA/W. This value is competitive with responsivity values extracted from published data for inorganic nanowires at irradiances similar to those used in this work: ~ 0.35 mA/W for a single InP nanowire device at low bias, and ~ 0.5 mA/W for a single ZnO nanowire device at 1 V bias. The quantum yield for the polymer nanowire device can also be estimated, as follows: The incident radiant energy delivered to the nanowire per second is $I_{irr}A \approx 5.10^{-7}$ J and the energy of a 405 nm photon is $E_p \approx 5.\ 10^{-19}$ J, thus yielding a flux ~ 10^{12} photons per second incident on the nanowire. The measured photocurrent ($I_{ph} \approx$ 200 pA) corresponds to ~ 10^9 carriers per second, yielding an external quantum efficiency ~ 0.1 %. Again, this is comparable to published data for single inorganic nanowires, where the

calculated external quantum efficiencies are ≈ 0.08 % and ≈ 0.17 % for single InP and ZnO nanowires, respectively. Overall, our results demonstrate the promise of these novel nanostructures as nanoscale building blocks with potential for integration into future hybrid nanophotonic devices and systems. In this regard, these nanostructures could form part of substrate-adaptive nanoarchitectures with novel photoconducting functionality.

Single nanowire laser

Tyndall also demonstrated photonic functionality in polyfluorene (PFO)-based nanowires processed using solution- and melt-assisted template wetting routes. They show a range of optical functions, from polarised emission to microcavity effects and single nanowire lasers. The work highlighted here reports on a single nanowire laser, which resulted from PFO nanowires that had been produced using the melt-assisted route. This route produced PFO nanowires with radial alignment of the emissive polymer molecules. This was achieved by careful control of anneal temperature, time and cooling rate during the synthesis. Photo-excited luminescence was polarized perpendicularly (radially) to the long axis of these wires as expected. Additionally, the radial molecular arrangement facilitated directional propagation of photoluminescence (i.e., active waveguiding) along the axis of single nanowires before out-coupling at the wire ends by diffraction. Further examination of the optical properties revealed that the nanowires were acting as optical cavities.

To investigate the possibility of the cavity acting as a laser, tip emission spectra were collected from isolated PFO nanowire microcavities as a function of pump energy; see ***figure 7a***. At lower pump energies, Fabry-Pérot modes were superimposed upon the broad PFO emission spectrum. Above a threshold incident pump energy of ~ 100 nJ (1.7 to 3.0 mJ/cm^2), a single spectrally narrowed emission peak with instrument-limited line width developed by preferential gain in a single Fabry-Pérot mode, characteristic of excitonic laser action. Concerning the dependence of tip emission intensity on pump energy, below threshold, emission increased linearly with excitation energy; see ***figure 7b***. Above threshold, a kink in emission output was followed by a super-linear increase due to optical gain. No such behaviour was observed at nanowire body locations indicating directional cavity output. While single mode lasing was common, multi-mode lasing was also occasionally observed. For 6 – 10 μm long PFO nanolasers, the threshold gain coefficient was between 4100 and 2800 cm^{-1} and the singlet threshold energy density was estimated to be 2 - 4 x 10^{19} cm^{-3}, similar to values reported during studies of planar PFO thin film waveguides and optical cavities.

This work resulted in a publication in *Nature Nanotechnology* with journal cover graphics: O'Carroll, D.; Lieberwirth, I & Redmond, G. *"Microcavity Effects and Optically Pumped Lasing in Single Conjugated Polymer Nanowires" Nat. Nanotech.* **2,** 180 (2007)

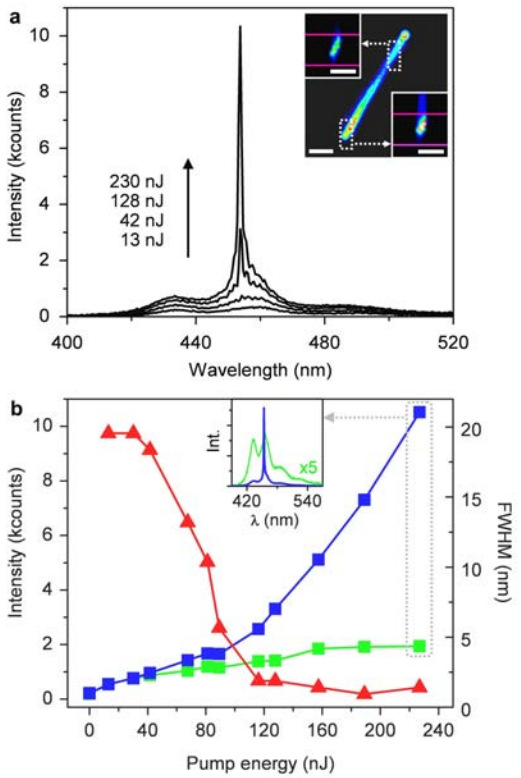

Figure 7. Optically pumped single PFO nanowire laser. (a) Emission spectra collected from the tip of an isolated PFO nanowire under uniform excitation as a function of increasing pump energy at room temperature. Inset: emission image of the wire (1.3 nJ) along with spatially filtered emission images of the tip and body locations from which spectral data was acquired. Scale bars, 2 μm. (b) Plot of the tip emission peak intensity (blue squares) and full-width-at-half-maximum (red triangles) versus pump energy for the wire shown in (a). The intensity of emission from the nanowire body (green squares) is low and almost linear with pump energy. Solid symbols correspond to experimental data points and lines are guides to the eye. Inset: above threshold (230 nJ) emission spectra acquired from the wire tip (blue) and body (green).

ADAPTIVE ARCHITECTURES

Wall and roof structures were prepared by casting copolymer solutions in photoresist structures followed by photocrosslinking of the copolymer (MPIP-MPG & UB with input from TNI-UCC). This addresses the objective of a three dimensional adaptive wall whose properties respond to a change in the environment.

Composite hydrogels consisting of a blend of pNiPAam (poly-*N*-isopropylacrylamide) and functionalised silica nanoparticles were prepared. Functionalisation and preparation conditions were designed such that the polymer and the nanoparticles could be homogeneously mixed and crosslinked well together. To optimise this model system in order to utilise it in both responsive wall and responsive roof
structures, the initial approach was to fabricate *integrated* roof and wall structures, as shown in ***figure 8***. Here, wall and roof are prepared simultaneously and responsiveness demonstrated for the integrated system.

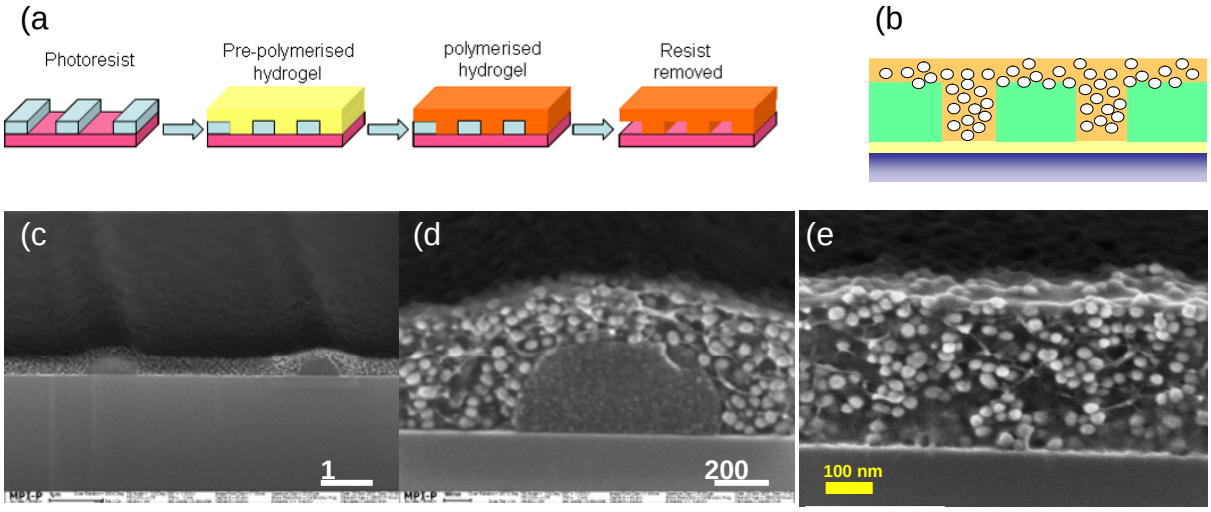

Figure 8. (a) Schematic depictions of the fabrication of an integrated roof and wall structure of pNiPAam (poly-*N*-isopropylacrylamide) and functionalised silica nanoparticles., (b) schematic cross section, (c)-(e) Cross-sectional SEM images of a wall+roof structure formed from a crosslinked blend of hydrogel and nanoparticles (2:1 weight ratio, 3.4 %-wt hydrogel) spin-coated from $CHCl_3$ at 5000 rpm and photocrosslinked.

The hydrogel matrix swells and collapses depending on the temperature: below the lower critical solution temperature (LCST, ca. 32°C) swelling occurs, above the LCST, the structure collapses. This was confirmed by temperature-dependent AFM measurements.

In order to exploit the substrate-responsive properties of the hydrogel-nanoparticle hybrid structures, a heating device based on Peltier-technology was constructed, which allowed anisotropic heating of the responsive wall- and roof structures. The experiment showed that it is indeed possible to get anisotropic collapse of the responsive channel structure during heating (see ***figure 9***).

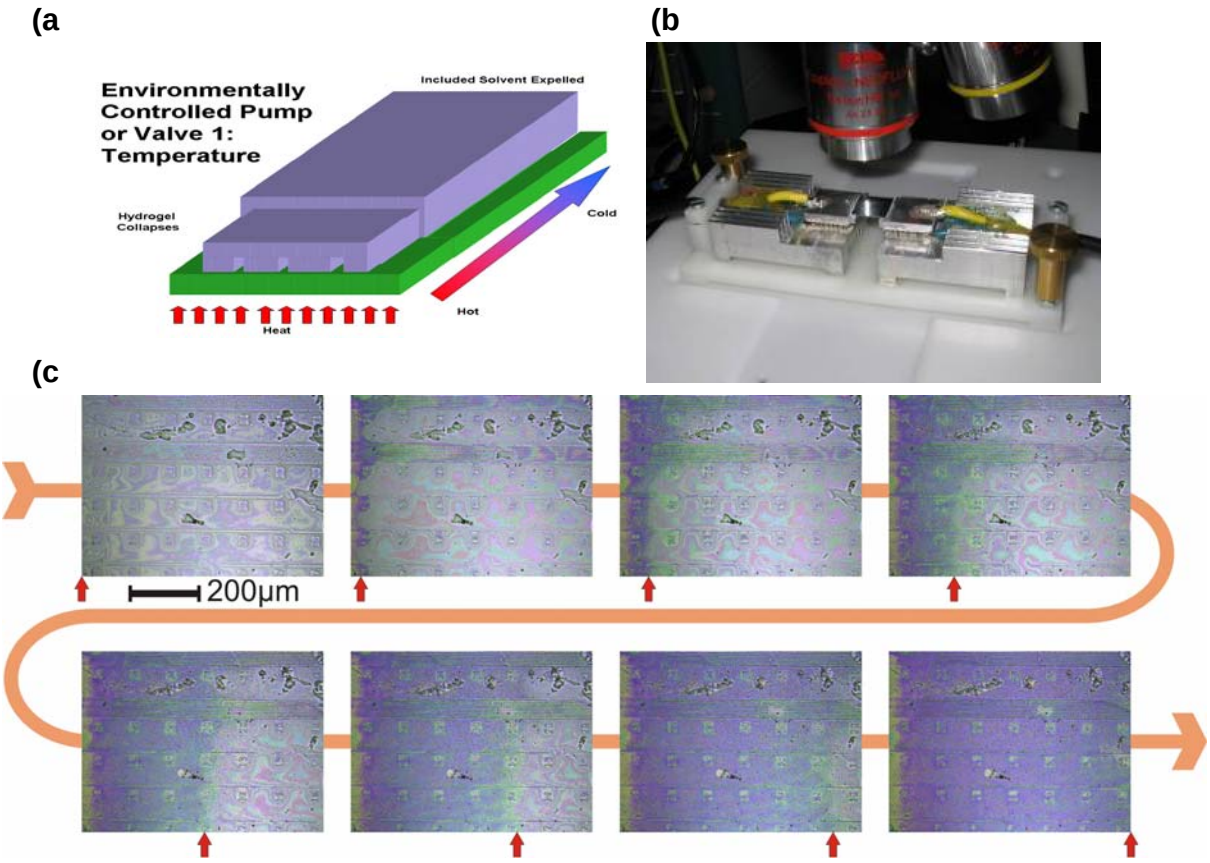

Figure 9. (a) Pump concept based on anisotropic heating and collapse of the hydrogel-nanoparticle hybrid channel structure. (b) Photograph of the anisotropic heating device on an optical microscopy stage constructed for the project. (c) Optical micrograph of the responsive channel structure during anisotropic heating (selection of images from a video sequence).

SCALE-UP

Two approaches were adopted for scale-up in the project, ink jet printing and microfluidics. The aim of this part of the project was to investigate the potential of these techniques to deliver materials and carry out processing at the *wafer scale*, rather than over the limited areas that most nanoscale processing has achieved to date. Both ink jet printing and microfluidics show promise for enabling the transfer of techniques developed in the project to larger scales, although there are difficulties inherent in both techniques.

Ink jet Printing

Following the development of the technique, a series of materials were deposited (jetted) at both 9D Technologies and the University of Birmingham:

Results from jetting monolayers

- Range of jetting weights
- PDAC polymer layers

- Hydrogel

Results from jetting multiple layers

- PDAC / Nanogold layers
- PDAC / Hydrogel structures

One example from such a multilayer structure is described and illustrated below for PDAC / hydrogel layers (Note: PDAC = polydiallyldimethylammonium chloride). Following work where hydrogel was spin coated onto a photoresist, it was shown that a model structure on the micron scale could be created by simultaneous ink jetting of walls and channel fillers, this was covered with a roof in a following step (see ***figure 10***).

From the model the idea was to jet hydrogel walls with a PDAC channel filler at the same time. After jetting a hydrogel roof on top, UV polymerisation of the roof and walls would make the structure insoluble, the PDAC channel "filler" could then be dissolved away in water. This was partially realized in a first step using a double structure where PDAC channel fillers were first jetted, then after drying covered with a hydrogel layer. UV polymerisation would allow the PDAC "fillers" to be removed from the hydrogel structure by dissolution in water. This would leave empty channels in the structure that will act as an adaptive pump, through the route of spin coating hydrogel onto photoresist then dissolving out the photoresist template (see ***figure 10***).

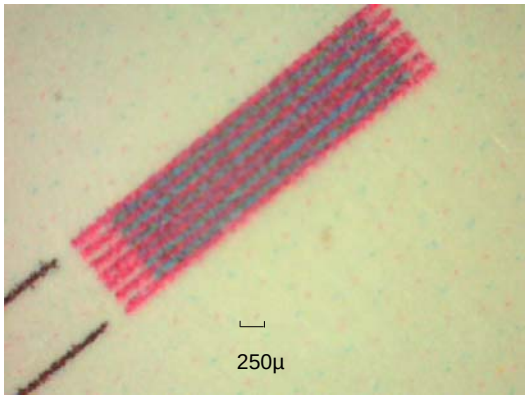

(a) Model walls + channel “fillers”

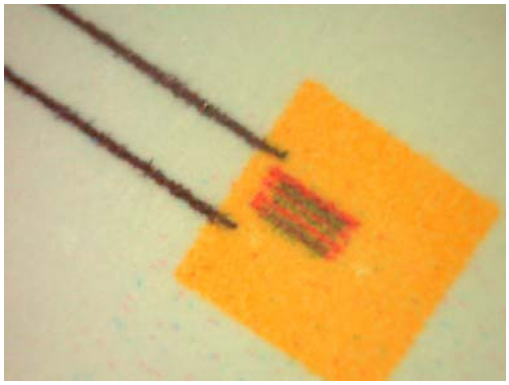

(b) Model walls + channel “fillers” covered with “roof”

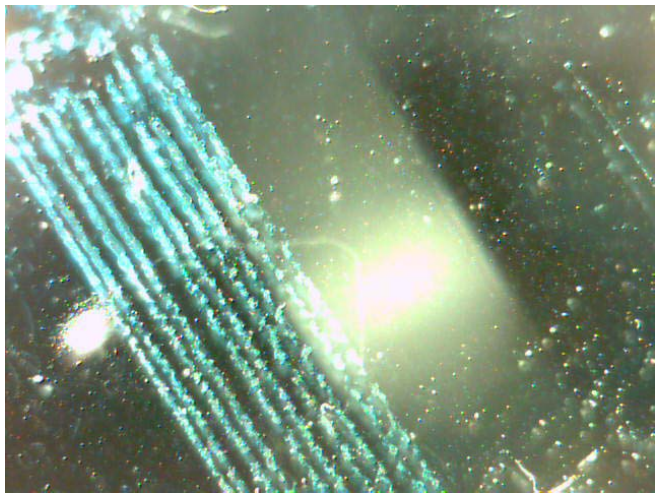

(c) PDAC channel “fillers” overprinted with 5x1Y hydrogel

Figure 10. (a) Model walls and channel fillers, (b) walls + channel fillers covered with roof, (c) PDAC channel fillers overprinted with hydrogel.

Microfluidics

The work described here summarises the activities to design and fabricate a microfluidic cell and the analysis of gold structures made using the cell.

The layout of the microfluidic cell design is shown in ***figure 11*** (inset: detail of delivery area). The completed cell comprises two wafers, the lower is a four-inch silicon wafer and an upper glass (pyrex) wafer forms the top part of the cell. The silicon wafer has a thermally grown oxide layer and a series of alignment and cell boundary marks patterned in sputtered metal. This forms an array of 5 x 5 cells each of which are 1 cm^2 in area and contain a processing area 80 μm x 80 μm. The microfluidic channels are created in the underside of the glass wafer, and deliver materials to the processing area (or delivery site). There are four microfluidic channels to each delivery site, allowing more than one material to be delivered to each site. The microfluidic channels were defined using a set of masks and a photoresist process, and were then created using powder blasting. A wet etch was used at the delivery site to create smoother structures in the glass, both for smoother liquid flow at this point and to enable optical inspection to be carried out. The

competed cell with ports attached is shown in ***figure 12***. Materials were delivered through these ports either by direct injection with a hypodermic syringe or in a controlled fashion using a syringe driver.

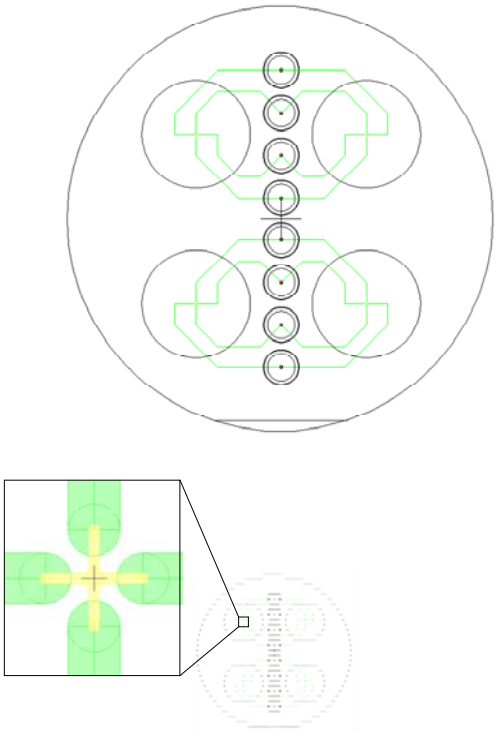

Figure 11. Detail of microfluidic cell layout. Microfluidic delivery sites are at intersections of green lines (channels). Large circles represent locations of microscope objective lens location for viewing structures build-up. Small (concentric) circles are locations of microfluidic delivery ports. Inset: detail of delivery site.

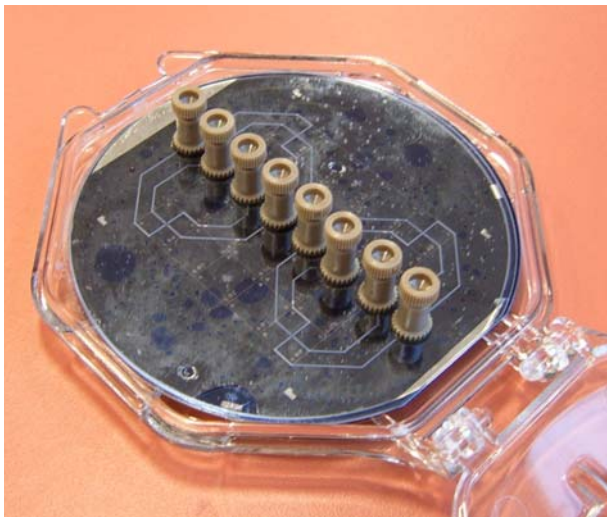

Figure 12. Completed microfluidic cell with delivery ports attached.

Gold nanoparticle structure deposition and layer build-up

A process developed in the *Building Blocks* work package was used to create structures on the silicon wafer surface. This involved the deposition of thiol-stabilised gold nanoparticles. The layers were deposited by spin-casting and were then exposed to UV light from a frequency-doubled argon ion laser, wavelength 244 nm. The exposure was done through a TEM grid to form a patterned structure. In regions where the nanoparticles were exposed to UV light, photooxidation occurs and the thiolate groups are converted to sulfonate groups. The latter were then removed with a chloroform rinse, leaving a pattern of the depassivated gold behind.

Following cell bonding, the gold structures were built up through microfluidic delivery. The process followed was as follows:

- Delivery of amino thiophenol. The thiol groups attach to the gold leaving protonated amino groups on the surface.
- Delivery of citrate-passivated gold nanoparticles. These attach to the amino groups through electrostatic interaction.
- Delivery of PDAC (poly-diallyldimethylammonium chloride) – this creates a protonated ammonium group which allows further citrate- passivated gold to be built up, and so on.

Figure 13 shows some representative results from the delivery of citrate passivated nanoparticles using the process decribed above. In ***figure 13a***, the striations appear after the introduction of the first batch of nanoparticles. After the second batch was introduced ***figure 13b***, the gold displays a colour change typically observed during the increase of thickness of such gold features. After the third introduction of nanoparticles in ***figure 13c***, a deeper gold colour was observed, along with striations across the cell which may be indicative of the fluid dynamics of the flow.

(a) (b) (c)

Figure 13. Gold nanoparticle delivery, (a) after first pass of nanoparticles, (b) second pass, (c) third pass.

These results show that it is possible to build up structures using microfluidics but that retaining any surface preparation, such as patterning, before the cell is fabricated is difficult. This is due to the harsh conditions encountered during preparation of the cell, notably the temperature required for satisfactory bonding, but also some of the commonly used cleaning and surface preparation methods are very aggressive.

Nevertheless these results do show that microfluidics could have a place in wafer-scale processing at the nanoscale for some materials, as there are other advantages such as the very small quantities of material employed and the ability to deliver materials precisely to multiple sites on a wafer simultaneously.

THE FUTURE

This project has not only demonstrated the feasibility of integrating top-down and bottom-up lithographic process, but also shown how the self-assembly of materials to these patterned surfaces can be automated *via* incorporation into ink-jet printing and microfluidic technologies. This capability is likely to be of significant relevance for the next generation nanotechnologies whereby conventional top-down approaches are not going to be scaleable.